Taylor & Francis
Taylor & Francis Group

Mechanics Based Design of Structures and Machines
An International Journal

ISSN: 1539-7734 (Print) 1539-7742 (Online) Journal homepage: http://www.tandfonline.com/loi/lmbd20

Normalization of the stress concentrations at the rounded edges of an interference fit between a solid shaft subjected to bending and a hub

Antonio Strozzi, Enrico Bertocchi, Andrea Baldini & Sara Mantovani

To cite this article: Antonio Strozzi, Enrico Bertocchi, Andrea Baldini & Sara Mantovani (2016) Normalization of the stress concentrations at the rounded edges of an interference fit between a solid shaft subjected to bending and a hub, Mechanics Based Design of Structures and Machines, 44:4, 405-425, DOI: 10.1080/15397734.2015.1086274

To link to this article: http://dx.doi.org/10.1080/15397734.2015.1086274

Accepted author version posted online: 22 Sep 2015.
Published online: 22 Sep 2015.

MECHANICS BASED DESIGN OF STRUCTURES AND MACHINES
2016, VOL. 44, NO. 4, 405–425
http://dx.doi.org/10.1080/15397734.2015.1086274

Taylor & Francis
Taylor & Francis Group

Normalization of the stress concentrations at the rounded edges of an interference fit between a solid shaft subjected to bending and a hub

Antonio Strozzi, Enrico Bertocchi, Andrea Baldini, and Sara Mantovani

Department of Engineering "Enzo Ferrari", University of Modena and Reggio Emilia, Modena, Italy

ABSTRACT

The elastic stress concentrations are addressed that are developed from the keyless frictionless press fit of a shaft subjected to bending into a hub with rounded bore edges. Derived from a formal modeling of the title problem in terms of an integral equation, a set of normalized parameters is proposed that accounts for the combined effects on the hub stress concentration of the fillet radius, the shaft radius, the hub outer radius, the hub axial length, the interference, the Young's modulus, and the bending couple. A numerical validation of the normalized parameters is presented. With the aid of Finite Elements, various design charts are compiled that (a) forecast the bending couple initiating the detachment between the shaft and the hub, and (b) report the elastic stress concentrations within the hub versus the proposed normalized parameters in the absence of shaft–hub detachment. Such charts assist the designer in dimensioning an interference fit in the presence of a bending couple.

ARTICLE HISTORY
Received 23 September, 2014
Accepted 20 August, 2015

KEYWORDS
Bending moment; contact stresses; finite elements; interference fit; normalizing parameters; shaft–hub detachment; stress concentration factor

1. Introduction

In this paper, the problem is examined of an interference fit between a hub with rounded bore edges and a solid shaft subjected to bending, see Fig. 1. The interference fit is assumed to be keyless and frictionless.

To limit the outcome of very high stress concentrations, the hub bore edges are generally rounded. The aim of this paper is three fold: (a) to examine the stress concentrations at the shaft-hub contact extremities in the vicinity of the rounded edges, concurrently promoted by the press fit and by the shaft bending; (b) to identify the variables that describe the situation of incipient detachment between the shaft and the hub as a result of the shaft bending; (c) to establish the normalized variables that rule the onset of the stress concentrations in the absence of shaft-hub detachment.

Such normalized variables ease the compilation of design charts that may assist the designer in avoiding an undesired detachment between the shaft and the hub, in forecasting the hub stress level in the absence of shaft-hub detachment, in predicting the possible outcome of yielding and in assessing the fatigue strength, and in selecting a convenient interval for the fillet radius of the rounded edges of the hub bore. It is underlined that the present paper addresses a traditional stress concentration problem, and that fretting fatigue aspects are only marginally touched upon; they constitute a topic beyond the scope of this paper.

This paper constitutes an extension of the works (Strozzi et al., 2011a, 2012), in which the hub stress concentrations originated by the press fit alone have been examined, whereas the effect of the application of a bending couple to the press fitted shaft has not been considered. This paper addresses only hub

CONTACT Enrico Bertocchi ebertocchi@unimore.it Department of Engineering "Enzo Ferrari", University of Modena and Reggio Emilia, Via Università, 4, 41121 Modena, Italy.
Color versions of one or more of the figures in the article can be found online at www.tandfonline.com/lmbd.
Communicated by Bahram Ravani.

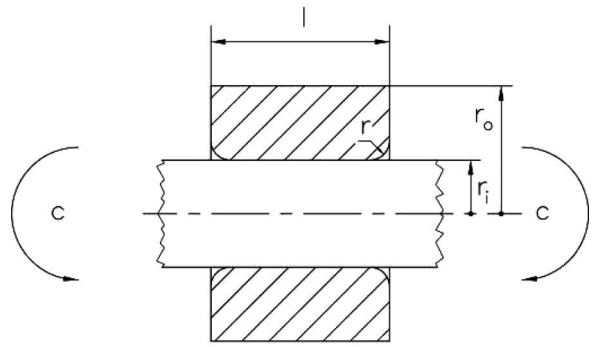

Figure 1. The shaft–hub assembly.

filleted edges shaped as a quarter of circle; filleted profiles shaped to achieve a more advantageous pressure distribution are considered in Strozzi et al. (2013).

The available salient information on the stress concentrations occurring in shaft-hub interference fits in the absence of bending couples is perfunctorily summarized in the following, see Strozzi et al. (2011a), for a solid shaft, and Croccolo et al. (2012) for the extension to a hollow shaft. Moving in the shaft axis direction, the contact pressure remains almost flat in the central zone of the shaft-hub contact, where it may be confidently evaluated with the Lamé equations for thick-walled cylinders; it exhibits Hertzian-type local bumps in the lateral zones where the hub bore edges are rounded; the contact pressure becomes null at the contact extremities. The lateral bumps and the central flattish zone confer to the contact pressure distribution a camel-backed profile. The peak equivalent stress in the shaft-hub press fit always occurs within the hub and not within the shaft, and it is located in the vicinity of the radiused edges of the hub bore. Consistent with the Hertzian nature of the pressure bumps, the maximum equivalent stress within the hub does not fall at the hub bore surface, but at a sub-superficial point.

In the following, the consequences on the press fit stress concentrations of the application of a bending moment to the shaft are addressed. The above bending moment confers a curvature to the shaft, which thus exhibits a concave and a convex side; it is conjectured in White and Humpherson (1969) and numerically proved in Garnett and Grimm (1989) that the shaft curvature modifies the stress field with respect to its counterpart addressing the press fit alone, by increasing (lowering) the lateral peak contact stresses in the shaft concave (convex) side. This result may be rationalized by observing that the shaft curvature increases the amount of compression exerted between the shaft and the hub extremities in the shaft concave side, thus enhancing the lateral peak contact stresses with respect to an unbent shaft. The stress field is no longer axisymmetric, but it becomes three-dimensional; as a result of the shaft rotation (the bending moment is supposed not to rotate with the shaft), the stresses are no longer steady as in Strozzi et al. (2011a), but they are subjected to a fatigue cycle. Unfortunately, although the Finite Element (FE) analysis carried out in Garnett and Grimm (1989) is considerably detailed, it assumes that the hub bore edges are sharp and, therefore, the stress forecasts are not immediately applicable to the title problem, in which the hub bore edges are rounded.

If the applied bending couple is sufficiently high, the shaft begins to detach from the hub in the hub bore edge proximity. A separation between the shaft and the hub contacting surfaces is highly undesired, since it promotes fretting between the mating surfaces. It is therefore technically interesting to evaluate the critical value of the bending couple that initiates the separation between the shaft and the hub. Although the separation problem is mentioned in the pertinent literature, *e.g.* Garnett and Grimm (1989), the present authors are unaware of the existence of diagrams or formulae forecasting the detachment initiation value of the bending couple. The only contribution loosely kindred to the present problem appears to be Hrylits'kyi and Krasnyuk (1997), where the axisymmetric, cylindrical problem of a pipe inserted into another pipe is considered, and the possible separation between the two

pipes as a result of an axisymmetric pressure distribution varying in the axial direction is explored in the framework of the theory of elasticity.

Since the above shaft-hub separation is undesired, the stress concentrations promoted by the combined effect of the interference fit and of the bending couple have been evaluated only in the absence of detachment.

It is finally observed that in the computations based on the standards DIN 7190, reported in GWJ Technology GmbH (2013), their Fig. 11.13, two external loadings superposed to the press fit stresses are considered, and simple design approaches are proposed to correct the stress state with respect to the axisymmetric state due to the shaft-hub press fit alone; such external loadings are (a) a bending couple applied to the hub, together with two radial forces (constituting an equilibrating couple) applied to the shaft, and (b) a transverse force applied to the hub, equilibrated by two radial forces applied to the shaft outside the hub length.

Although the above loadings are practically as interesting as the loading depicted in Fig. 1, they are described by a higher number of variables. In particular, the position of the application of the equilibrating loads must be accounted for, and, therefore, results of ample validity are more difficult to achieve. The above loadings are not treated in this paper, and they are not depicted here to avoid confusion.

Several additional works investigate a shrink fit assembly subjected to rotating bending, but mainly from the viewpoint of the growth of fretting fatigue cracks, e.g. Lee et al. (2006); Gutkin and Alfredsson (2008); Madia et al. (2008).

The main aim of this paper is to identify the normalized variables that rule the onset of the stress concentrations in the absence of surface separation between the shaft and the hub. In fact, the intensity of the contact pressure bumps, and the corresponding stress concentrations due to the combined effects of a press fit and a shaft bending, depend on seven dimensional variables, namely the shaft radius, the hub outer radius, the hub axial length, the fillet radius, the interference, the bending couple applied to the shaft, and the hub and shaft Young's moduli, see Fig. 1 for the definition of most of the symbols. Since the number of variables to be simultaneously considered is appreciable, it is a demanding task to organize complete design charts or to derive formulae of ample validity, suitable for forecasting the hub stress concentrations. A regrouping of the above variables, capable of reducing the number of independent variables and, hopefully, of evidencing the more important parameters, is therefore desirable.

In this paper, the leading seven variables are regrouped to define five dimensionless parameters that dictate the outcome of the stress concentrations, whose rationale is presented in Section 3 by formally casting the title problem in terms of an integral equation. The relative influence of the five adimensional parameters is explored. A table compiled with the aid of FE, confirming the validity of the normalizing parameters, is presented in Section 5. Diagrams quantifying the situation of incipient detachment between the shaft and the hub are reported in Section 6. Design diagrams compiled for situations of absence of shaft-hub detachment, that are useful for the dimensioning of an interference fit, are reported in Section 7, and their applicability to fatigue stress cycles is discussed in Section 8.

2. Simplifying assumptions

Most of the assumptions made in Strozzi et al. (2011a), and commonly accepted in the mechanical analysis of shaft-hub press fits, are adopted in the present study.

It is assumed that the rounded edges of the hub bore, see Fig. 1, are described by a quarter of circumference. Consequently, the fillet radius fully describes the geometry of the mating surfaces at the hub-shaft contact.

The shaft is assumed to protrude from the hub by a sizeable length, so that the effect on the shaft-hub contact stresses of the shaft extremities is insignificant with respect to an infinitely long shaft.

The shaft is supposed to be solid.

The materials of the shaft and of the hub are assumed to behave elastically and to exhibit the same Young's modulus. The Poisson's ratio is assumed to possess the commonplace value 0.3.

The shaft-hub contact is modeled as frictionless.

The shear stresses connected to the torque transmission are neglected; the inertial forces due to the shaft rotation are ignored.

It is finally assumed that an interference fit is always present, whereas the bending couples applied to the shaft may be absent. The bending moment is assumed not to rotate with the shaft.

3. Formal modeling in terms of an integral equation

In this section, the normalized variables that rule the onset of the stress concentrations in the absence of shaft-hub detachment are derived by formally casting the title problem in terms of an integral equation. Figure 1 illustrates the geometry of the title problem, and it clarifies the meaning of the majority of the seven variables defining the problem under scrutiny. Such variables are the shaft radius, r_i, the hub outer radius, r_o, the hub axial length, l, the fillet radius at the hub bore edge, r, the diametral interference of the shaft-hub fit, I, and the bending couple applied to the shaft projecting extremities, C. The hub inner radius nominally coincides with the shaft radius, r_i. The Young's modulus of the shaft and the hub is denoted by E.

The above seven independent variables may be regrouped on a mathematical basis to achieve composed, normalized parameters. However, a favorable regrouping of the leading variables, evidencing the most influential terms, may only stem from a physical description of the contact mechanism. To this aim, the title problem is formally cast in terms of an integral equation.

However, following Strozzi et al. (2011a), instead of considering the actual problem depicted in Figs. 1 and 2(a) and (b) (for simplicity, the drawings of Fig. 2(a) and (b) refer to the situation of null bending couple), the closely related, more manageable problem of Fig. 2c–f is examined. In this simplified problem, the whole hub bore border is rounded, whereas in the actual problem (see Figs. 2(a) and (b)) the bore border is described by a flat zone surrounded by two rounded portions. With this simplification, there is no need to treat separately the flat and rounded parts of the hub profile, and the single Eq. (2) below describes the initial overlapping/clearance along the whole shaft-hub contact width, see also Eq. (7) of Ciavarella et al. (1998). It has been shown in Strozzi et al. (2011a) that the normalized variables derived from the simplified problem of Fig. 2(c) and (d) are valid for the actual geometry too. The integral equation expresses the imposition that the contact pressure, p, must move apart the mating surfaces of the shaft and of the hub bore, until they do not overlap, under the restriction that the contact pressure be positive or null. The unknown function is the contact pressure, p, appearing under integration at the left-hand side of the integral equation, whereas the right-hand side is the known term, representing the initial overlapping/clearance between the two undeformed surfaces of the shaft and of the hub.

The modeling of the left-hand side containing the unknown contact pressure, p, is examined first. The Green function, k, describes the relative radial displacement at the axial, z, Fig. 2(c) and angular, θ, Fig. 2(f), coordinates of the two shaft-hub mating profiles for a concentrated radial force applied at the axial, z', Fig. 2(c), and angular, ω, Fig. 2(f), coordinates. In addition, r_i denotes the shaft radius. In other words, in agreement with the integral equation formulation favored in this study, the variables z' and ω are inner, dummy variables, whereas z and θ are outer variables.

Accordingly, the left-hand side of the integral equation is

$$\int_{\Omega} k\left(z, z', \theta, \omega\right)\ p\left(z', \omega\right) r_i\ d\omega\ dz' \tag{1}$$

where Ω denotes the extent of the contact zone between the shaft surface and the hub bore surface, expressed in terms of the axial, z', and angular, ω, coordinates.

The modeling of the initial overlapping/clearance is examined in the following. For an unbent shaft, the initial radial interference, g, between the shaft surface and the plate bore surface is, *e.g.* Johnson

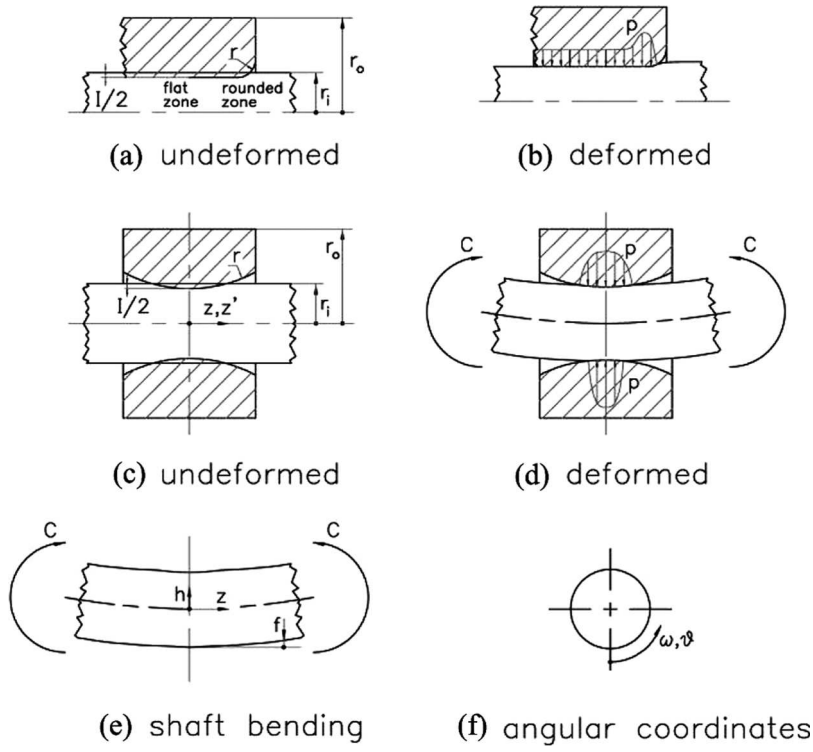

Figure 2. Simplification of the contact problem.

(1987) and Ciavarella et al. (1998).

$$g(z) = \frac{I}{2} - r + \sqrt{r^2 - z^2} \tag{2}$$

where I indicates the diametral interference, r denotes the radius of the hub bore rounded edge, and z is the axial coordinate, whose origin is at the hub centre, Fig. 2(c).

The shaft bending caused by the two bending couples, C, produces a radial displacement, f, Fig. 2(e), of the shaft surface that may be evaluated with the classical beam theory. The expression of f is

$$f(z,\theta) = \frac{C}{2EJ_s} z^2 \cos\theta \tag{3}$$

where, again, z denotes the axial coordinate, and θ the angular coordinate, whose origin falls at the midpoint of the shaft convex side, Fig. 2(f). In addition, J_s is the moment of inertia of the shaft circular cross section, and E is the Young's modulus common to the shaft and hub materials.

A further term for the radial displacement, that accounts for a shaft vertical rigid translation, e, relative to the hub, needs to be added to the previous Eqs. (2, 3). This translation modifies the contact pressure until the shaft vertical equilibrium is satisfied. The corresponding radial displacement, h, Fig. 2(e), is

$$h(\theta) = e\cos\theta \tag{4}$$

where e remains constant with the axial position.

By employing the previous Eqs. (1–4), the integral equation becomes

$$\int_\Omega k\left(z,z',\theta,\omega\right)\ p\left(z',\omega\right)\ r_i\, d\omega\, dz' = \frac{I}{2} - r + \sqrt{r^2 - z^2} + \frac{C}{2EJ} z^2 \cos\theta + e\ \cos\theta \tag{5}$$

4. Simplification and normalization of the integral equation

It is difficult to determine the analytical expression of the Green function k, especially for the hub, since its axial length is finite, and to analytically solve the integral Eq. (5). However, by evidencing the properties of k, and by introducing some simplifications and normalizations, the integral equation may be given a more compact expression, that provides useful information on a physically-based regrouping of the leading variables.

As a first observation, the function k may be expressed in terms of coordinates normalized with respect to a representative dimension of the press fit, for example the shaft radius, r_i. Second, the Green function is inversely proportional to r_i and to the Young's modulus E common to the two materials of the shaft and the hub. Therefore

$$k\left(z,z',\theta,\omega\right)=\frac{\bar{k}}{r_iE}\left(\frac{z}{r_i},\frac{z'}{r_i},\theta,\omega\right) \tag{6}$$

where $\bar{k}$ is a normalized Green function referring to a unit shaft radius and a unit Young's modulus.

The initial radial interference, g, between the shaft surface and the hub bore surface, see Eq. (2), may be simplified by adopting the classical Hertzian-type, parabolic approximation, *e.g.* Strozzi et al. (2011a)

$$g\left(z\right)=\frac{I}{2}-\frac{z^2}{2r} \tag{7}$$

By employing Eqs. (6, 7), the integral equation (5) becomes

$$\int_\Omega \frac{\bar{k}}{r_iE}\left(\frac{z}{r_i},\frac{z'}{r_i},\theta,\omega\right)\ p\left(z',\omega\right)\ r_i\ d\omega\ dz'=\frac{I}{2}-\frac{z^2}{2r}+\frac{C}{2EJ}z^2\cos\theta+e\ \cos\theta \tag{8}$$

The shaft vertical rigid translation, e, may be exactly computed by solving the integral Eq. (8) in terms of the contact pressure and of e, and by imposing the vertical equilibrium condition for the shaft. This approach being prohibitively complex, an approximate evaluation of e may be achieved by assuming that the distribution of the contact pressure, p, be approximately proportional to the known term of the integral equation, expressing the initial radial clearance/overlapping between the shaft and the hub, and by formulating the vertical equilibrium condition for the shaft in terms of this approximate pressure distribution, which depends on e.

The assumption of the contact pressure being proportional to the known term of the integral equation is consistent with a Winkler-type approximation (see Antoni, 2014 for a comparable application), and it is expected to be acceptable in the central part of the contact, where the contact pressure varies smoothly; instead, this approximation will become appreciably poorer in the vicinity of the pressure bumps, characterized by high gradients, (see Croccolo et al., 2012; Strozzi, 2012; Strozzi and Bertocchi, 2015). However, since these latter contact portions are relatively small, their contribution to the shaft vertical equilibrium condition is deemed to be limited with respect to that of the central part of the contact.

Moving to the formulation of the shaft vertical equilibrium equation, the following simplified approach is adopted. The integration of the vertical component of the contact pressure in the z direction is carried out along the whole hub length, l, i.e., the (narrow) zones are included in which the shaft-hub contact is physically absent as a result of the presence of the rounded edges. Consequently, the shaft vertical equilibrium requires that

$$\int_{-l/2}^{l/2}\int_{-\pi}^{\pi}\left(\frac{I}{2}-\frac{z^2}{2r}+\frac{C}{2EJ_s}z^2\cos\theta+e\ \cos\theta\right)\cos\theta\ dz\ r_i\ d\theta=0 \tag{9}$$

which produces the following approximate value for e

$$e=-\frac{Cl^2}{24EJ_s} \tag{10}$$

The numerical results of Section 5 confirm the validity of the above procedure. By inserting the above value for e into the integral Eq. (8) one finally obtains

$$\int_{\Omega} \frac{\bar{k}}{r_i E}\left(\frac{z}{r_i},\frac{z'}{r_i},\theta,\omega\right)\, p\left(z',\omega\right)\; r_i\, d\omega\, dz' = \frac{I}{2} - \frac{z^2}{2r} + \frac{C}{2EJ_s}z^2\cos\theta - \frac{Cl^2}{24EJ_s}\;\cos\theta \tag{11}$$

The main aim of the development of the integral formulation (11) of the title problem is not to provide the contact pressure profile, but to suggest how to regroup the leading variables in a physically sound manner. Instead, the evaluation of the contact pressure profile is relegated to FE.

The following passages aim at normalizing the two sides of the integral Eq. (11), in order to define the normalized parameters that rule the title problem. The contact pressure p may be normalized with respect to the reference contact pressure p_0, computed by ignoring the presence of the bending couple, C, by modeling the press fit problem as plane (polar), and by employing the classical Lamé equations for thick-walled cylinders. Consistent with the above normalization, in the definition of the stress concentration factor K_t, the contact pressure p_0 has been assumed as the normalizing parameter. The reference contact pressure p_0 describes the contact pressure along the central portion of the actual shaft-hub press fit, in the absence of the bending couple, C (recalling that the diametral interference I is assumed to be non-null, whereas the bending couple C may be null), and it may be expressed in terms of the diametral interference I, the shaft radius, r_i, and the hub radial aspect ratio, see *e.g.* Strozzi et al. (2011a)

$$p_0 = \frac{EI}{2r_i}\frac{1}{1+\frac{r_i^2+r_o^2}{r_o^2-r_i^2}} = \frac{EI}{4r_i}\left(1-\frac{r_i^2}{r_o^2}\right) = \frac{EI}{r_i}\left[\frac{1}{4}\left(1-\frac{r_i^2}{r_o^2}\right)\right] = \frac{EI}{r_i}F\left(\frac{r_i}{r_o}\right) \tag{12}$$

where $F(r_i/r_o)$ denotes the function $(1-(r_i/r_o)^2)/4$. By normalizing p over p_0, the integral Eq. (12) may be recast as

$$\int_{\Omega} \frac{\bar{k}}{r_i E}\left(\frac{z}{r_i},\frac{z'}{r_i},\theta,\omega\right)\,\frac{p\left(z',\omega\right)}{p_0}\; r_i\, d\omega\, dz' = \frac{r_i}{EI\; F\left(\frac{r_i}{r_o}\right)}\left(\frac{I}{2} - \frac{z^2}{2r} + \frac{C}{2EJ_s}z^2\cos\theta - \frac{Cl^2}{24EJ_s}\;\cos\theta\right) \tag{13}$$

or, after some manipulations, as

$$\int_{\Omega} \bar{k}\left(\frac{z}{r_i},\frac{z'}{r_i},\theta,\omega\right)\,\frac{p\left(z',\omega\right)}{p_0}\; d\omega\, d\left(\frac{z'}{r_i}\right) = \frac{1}{2F\left(\frac{r_i}{r_o}\right)}\left[1-\left(\frac{z}{r_i}\right)^2\frac{r_i^2}{I\,r} - \frac{C\,l^2}{12IEJ_s}\left(1-12\left(\frac{z}{r_i}\right)^2\left(\frac{r_i}{l}\right)\right)\cos\theta\right] \tag{14}$$

An attentive examination of the normalized integral Eq. (14) indicates that the normalized pressure, p/p_0, may be expressed in terms of four normalized variables, namely r_i/r_o, $r_i^2/(Ir)$, $Cr_i^2/(\text{IEJs})$, r_i/l. It should, however, be noted that the above analysis ignores the effect of a further parameter. In fact, the above normalized parameters stem from an integration carried out in the z' variable up to the contact extremities, and, therefore, they do not account for the hub projections beyond the contact zone, whose presence increases the hub radial stiffness, see Strozzi et al. (2011a) for details, and Strozzi et al. (2014) for the plane counterpart of the problem. Consequently, a fifth normalized variable must be added to the previous list, namely r/r_i. In Strozzi et al. (2011a)—in the absence of bending couple, it is shown that the effect of this parameter is generally limited, and this property is deemed to be valid for the title problem too, *i.e.* in the presence of bending couple. It is concluded that the normalization procedure favored in this paper has lowered the initial seven independent variables to five normalized parameters, amongst which r/r_i is expected to be of limited relevance.

5. Numerical validation of the normalized parameters

To assess whether the normalized pressure, p/p_0, and, more generally, the stress concentration factor, K_t, depend exclusively upon the five normalized variables Ir/r_i^2, r_i/r_o, r_i/l, r/r_i, $Cl^2/(\mathrm{IEJs})$, a mechanical analysis of two different shaft-hub assemblies, named Case 1 and Case 2, has been carried out with the aid of FE, and the numerical forecasts have been collected in Table 1.

The commercial FE program MSC Marc 2013 has been employed in this study to determine the stress values. The 3D mesh is formed by about 670,000 nodes, whose element size grades smoothly from 2.2e-5 to 0.1 times r_i. The nodes in contact between the shaft and the hub rounded edges in the axial direction are more than ten, as suggested in the pertinent literature, see Strozzi et al. (2011a). In some test cases, an even finer mesh was employed to assess the numerical convergence. The symmetry of this problem was exploited to contain the number of nodes. Particular attention was paid to ease the convergence of the unilateral contact algorithm by preventing the problems deriving from the sliding and the resulting misalignment of the initially facing nodes in the finely meshed contact areas. Additional details are omitted for brevity.

In Fig. 3, the hub is located in the upper part, and the equivalent stress reaches its maximum within the hub, in the vicinity of the rounded zone.

Table 1. Comparison between two test cases exhibiting different geometries but characterized by the same values of the normalizing parameters.

	Case 1	Case 2
hub inner radius, r_i	20 mm	15 mm
hub inner radius, r_o	40 mm	30 mm
fillet radius, r	1 mm	0.75 mm
hub length, l	100 mm	75 mm
diametral interference, I	0.04 mm	0.03 mm
Young's modulus, E	210000 MPa	100000 MPa
applied couple, C	660 Nm	132.6 Nm
Ir/r_i^2	0.0001	0.0001
r_i/r_o	0.5	0.5
r_i/l	0.2	0.2
r/r_i	0.05	0.05
$Cl_2/(\mathrm{IEJs})$	1.563	1.563
p_0	78.75 MPa	37.5 MPa
$\sigma_{\mathrm{eq,max}}$	833.4 MPa	396.8 MPa
$K_t = \sigma_{\mathrm{eq,max}}/p_0$	10.583	10.581
K_t antipodal to the previous one	4.618	4.619
K_t for $C = 0$	7.873	7.872

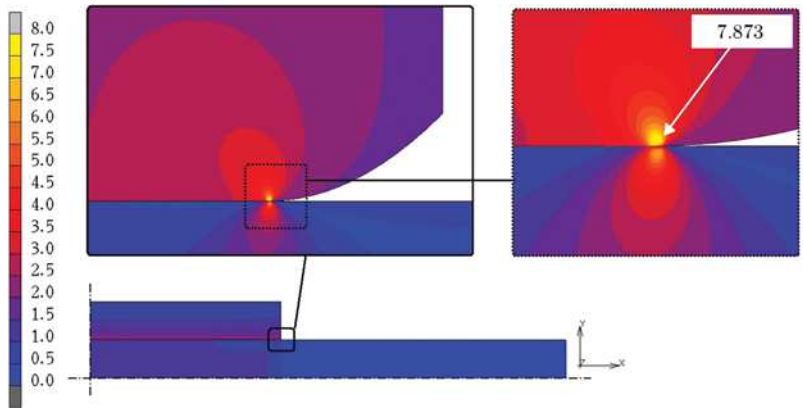

Figure 3. The FE equivalent stress field, normalized with respect to the reference contact pressure p_o.

The shaft radius r_i (nominally coinciding with the hub bore radius), the hub outer radius, r_o, the radius of the hub bore edge, r, the hub length, l, the diametral interference, I, the Young's modulus, E, and the bending couple, C, are different for the two Cases. However, the five dimensionless parameters Ir/r_i^2, r_i/r_o, r_i/l, r/r_i, $Cl^2/(\text{IEJs})$, are the same for the two Cases.

Table 1 reports the stress concentration factor K_t, defined as the hub maximum von Mises equivalent stress, $\sigma_{eq,max}$, normalized with respect to the reference contact pressure p_0 incorporating the Young's modulus effect. To provide information on the stress fluctuation during the shaft rotation, Table 1 also includes the value of K_t antipodal to the previous one, defined as the hub local maximum equivalent stress in an angular position antipodal to that in which the absolute maximum equivalent stress occurs, normalized over the reference contact pressure p_0. Finally, the maximum equivalent stress for a null couple has also been included, to supply data on the relative relevance of the shaft bending effect.

Encouragingly, Table 1 confirms the analytical expectations according to which, for different dimensions of the shaft and the hub, different fillet radii and initial clearances, and different Young's moduli, but for equal values of the above five normalized parameters, the normalized maximum equivalent stress remains (essentially) the same. These results also support the validity of the procedure adopted for the evaluation of e in Eqs. (9) and (10). The tabulated values of K_t for null couple C are very close to the value 7.833 computed with the interpolating formula of Strozzi et al. (2012). Finally, the numerical forecasts referring to the angular position antipodal to the maximum stress show that the stress fluctuations may be relevant.

6. The shaft–hub detachment

If a press fit is considered in which the hub bore edges are either rounded or sharp, and the bending couple C is absent, the shaft-hub contact extent is axisymmetric. Conversely, when a bending couple is applied to the shaft press fitted into the hub, the shaft bends, and the contact stresses lose their axisymmetry. In particular, moving circumferentially along a contact extremity region, the contact pressure at the shaft-hub contact extremities is higher (lower) in the shaft concave (convex) side, see the Introduction of this paper, and Garnett and Grimm (1989); the shaft-hub detachment begins in the extremal zones at the shaft convex side, when the bending couple is sufficiently high to counterbalance the press fit contact pressure. Instead, no detachment takes place in the contact central, antipodal regions for the geometries examined.

It would be conceivable to employ the five normalized variables defined in Section 4 to compile FE design charts summarizing the combinations of the variables that initiate the shaft detachment from the hub in the presence of rounded edges in the hub bore, Fig. 4(a). This task being particularly demanding, it was decided, following Garnett and Grimm (1989), to refer to a hub with sharp edges, Fig. 4(b), thus neglecting the effect of the rounded edges in the definition of the critical couple. With this simplification, the independent normalized parameters reduce to three, namely $Cr_i^2/(\text{IEJs})$, r_i/r_o, r_i/l.

It is additionally noted that the sharp edge assumption permits a mechanically sound definition of the bending couple initiating the shaft-hub detachment. In fact, the (finite) value of the bending couple

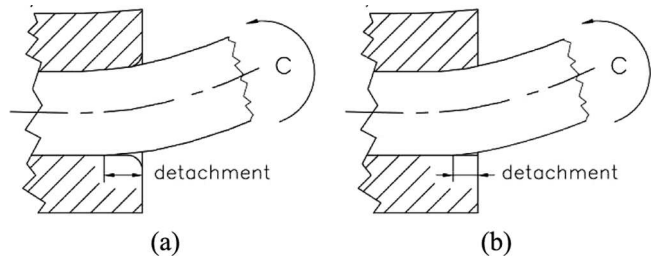

Figure 4. The shaft–hub detachment in the cases of (a) filleted hub bore edge; (b) sharp hub bore edge.

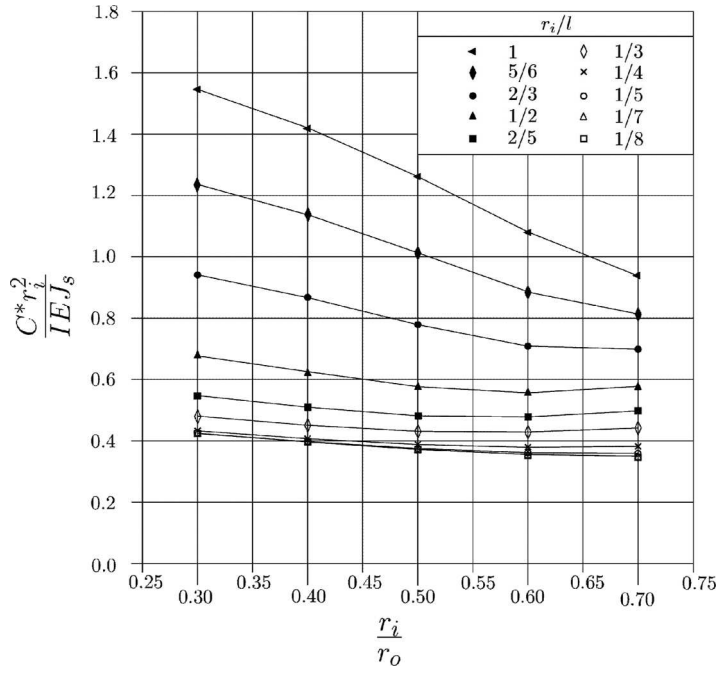

Figure 5. The value of $C^* r_i^2/(\text{IEJs})$ versus r_i/r_o for a selection of r_i/l values, in the situation of incipient shaft–hub detachment. The hub edges are sharp.

is sought that annuls the press fit pressure. Instead, when the hub bore edges are rounded, a vanishingly small bending couple produces a shaft curvature causing a moderate regression, at the shaft convex side (see the Introduction), of the contact extent in the shaft axial direction; as the bending couple increases, the hub bore filleted portion detaches first, and, upon a further increase of the bending couple, the detachment zone reaches the initially flat portion of the hub bore axial profile; mathematically, this continuously regressive behavior indicates that the shaft-hub detachment is initiated by a vanishingly small bending couple; from an engineering viewpoint, instead, a value is sought of the bending couple that constitutes a sound indicator of a significant shaft-hub detachment. A mechanically sound definition of the beginning of the shaft-hub detachment in the presence of hub bore filleted edges is proposed below; this definition stems from a comparison of the detachment evolution between sharp-edged and round-edged hub bores, see Fig. 6 below.

A FE campaign has been carried out, and the forecasts of the bending couple initiating the detachment in the presence of sharp edges have been collected in Fig. 5. This Figure reports the variable r_i/r_o along the x-axis, and the variable $C^* r_i^2/(\text{IEJs})$ along the y-axis, where C^* denotes the critical value of the bending couple that initiates the shaft-hub detachment. The ten curves refer to a selection of r_i/l values, namely $r_i/l = 1/8, 1/7, 1/5, 1/4, 1/3, 2/5, 1/2, 2/3, 5/6, 1$, and they express the combination among the three above variables that causes a situation of incipient shaft-hub detachment.

The curves referring to $r_i/l \leq 1/4$ are essentially superposed, thus indicating that for such shape ratios the hub length becomes marginally influential. In addition, since such curves are essentially horizontal, the effect of the ratio r_i/r_o is limited too. Therefore, for sufficiently long hubs ($r_i/l \leq 1/4$) and for usual r_i/r_o ratios ($0.3 \leq r_i/r_o \leq 0.7$), the normalized expression $C^* r_i^2/(\text{IEJs})$ of the critical bending couple C^* that initiates the shaft-hub detachment in a sharp-edged hub, constitutes a favorable normalization, since it allows the formulation of the remarkably simple equation

$$\frac{C^* r_i^2}{IEJ_s} \approx 0.4 \tag{15}$$

to forecast the critical value of the bending couple that initiates the shaft-hub detachment in a sharp-edged hub.

The curves referring to $2/3 \leq r_i/l \leq 1$ decrease when r_i/r_o, increases, thus giving the physically unjustified impression that, for a prescribed hub outer radius r_o, the value of the critical bending couple C^* that initiates the shaft-hub detachment in a sharp-edged hub decreases as r_i increases. To clarify this aspect, the trend of the curve referring to $r_i/l = 1$ is examined in detail in the following. Within the interval $0.3 \leq r_i/r_o \leq 0.7$, this curve may be approximated by the following linear equation

$$\frac{C^* r_i^2}{IEJ_s} \approx 2 - 1.5\frac{r_i}{r_o} \tag{16}$$

By introducing the expression of J_s in terms of the shaft radius r_i, Eq. (16) becomes:

$$\frac{C^* r_i^2}{IE\frac{\pi}{4}r_i^4} \approx 2 - 1.5\frac{r_i}{r_o} \Rightarrow \frac{4C^*}{\pi IEr_o^2} \approx \left(2 - 1.5\frac{r_i}{r_o}\right)\left(\frac{r_i}{r_o}\right)^2 \tag{17}$$

The last equation shows that, for a prescribed value of the hub outer radius r_o, the above critical value of C^* triplicates when the ratio r_i/r_o increases from 0.3 to 0.7. In conclusion, although, for a prescribed hub outer radius r_o, the normalized parameter $C^* r_i^2/(\text{IEJs})$ decreases as r_i increases, the value of the critical bending couple C^* increases with r_i. An increase of C^* with r_i/r_o is expected on physical grounds.

It is difficult to discuss, for a general shaft-hub assembly, the applicability to a hub with filleted bore edge of the detachment forecasts in terms of the critical bending couple of Fig. 5, referring to a sharply edged hub bore. Some indications are provided by the following selected example. In the presence of hub bore fillets, a suitable definition of the shaft-hub detachment initiation is the beginning of the detachment of the initially flat portion of the hub bore axial profile.

Figure 6 addresses a geometry defined by $r_i/r_o = 0.5$, $r_i/l = 0.5$ and $I/r_i = 0.02$; three normalized fillet radii have been considered, namely $r/r_i = 0, 0.025, 0.05$. The x-axis reports the parameter $C/C^* - 1$

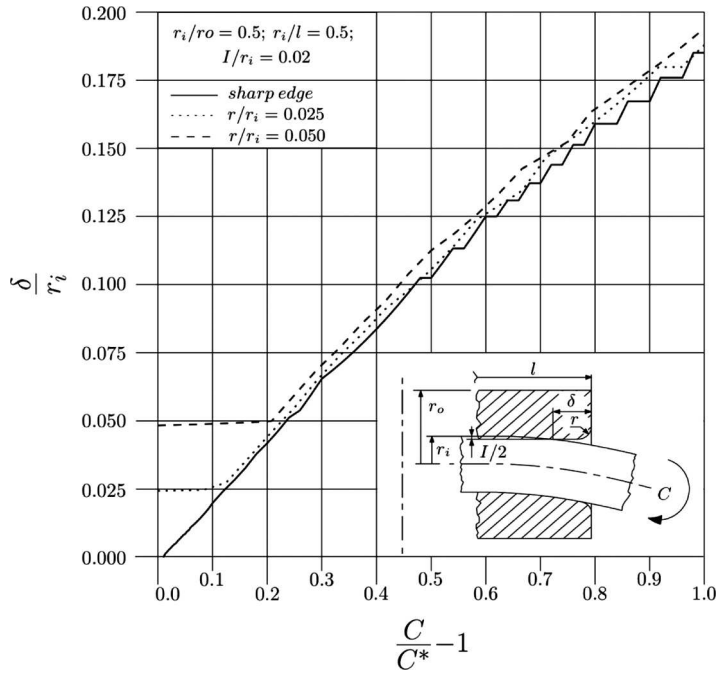

Figure 6. The normalized detachment extent δ/r_i versus $C/C^* - 1$ for $r_i/r_o = 0.5$, $r_i/l = 0.5$, $l = 0.02r_i$ and for the three normalized fillet radii $r/r_i = 0, 0.025, 0.05$.

quantifying the normalized surplus of the applied couple C beyond its critical value C^* computed for a sharp edge; the y-axis reports the normalized axial extent of the shaft-hub detachment, δ/r_i, measured from the hub lateral faces.

In the case of the sharp edged geometry (described by a solid curve), the detachment extent progresses essentially linearly with the bending couple value exceeding its critical threshold, up to levels of the bending couple twice its critical value. Moving to the two curves referring to non-null filleted edges of the hub bore (described by dotted and dashed curves), the detachment zone extent does not start from the origin, but from a value essentially coinciding with the fillet radius, since along this zone the hub is initially (*i.e.*, when $C = C^*$) detached from the shaft, apart from the extent of the compressed filleted region. When the detachment zone reaches the initially flat portion of the hub axial profile, the three curves become essentially superposed.

The moderate offset of the solid curve with respect to the diagram origin is due to numerical approximations in exactly defining the detachment initiation of the first node. The wiggles perceivable for high values of the x-variable are due to the detachment extent reaching zones where the mesh adopted is coarser.

Figure 6 shows that for the geometry defined by $r/r_i = 0.025$ the detachment initiation requires $C/C^* - 1 \approx 0.1$, that is, the couple C that initiates the detachment for the filleted geometry must exceed by 10% its critical value C^* referring to a sharp edge. Similarly, for the geometry defined by $r/r_i = 0.05$ the detachment initiation requires $C/C^* - 1 \approx 0.2$, that is, the couple C initiating the detachment for the filleted geometry must exceed by 20% its critical value C^* referring to a sharp edge. It may be concluded that the critical couple forecasts of Fig. 5, referring to a sharp edged hub, provide a minorant of the detaching couple for a round edged hub, and, therefore, they supply design information useful for preventing a possible detachment in a shaft-hub assembly with filleted hub bore edges too.

7. Design diagrams

Design charts addressing the stress concentrations in the absence of shaft-hub detachment may assist the designer of a press fitted assembly in selecting the most convenient fillet radius, in evaluating the maximum equivalent stress, and in assessing its fatigue strength and the possible outcome of yielding.

Design diagrams are technically conceivable that report the hub stress concentration factor for wide intervals of the five dimensionless parameters Ir/r_i^2, r_i/r_o, r_i/l, r/r_i, $Cr_i^2/(\text{IEJs})$. However, although the normalization procedure favored in this paper succeeded in reducing the initial seven independent variables to five normalized parameters, the compilation of exhaustive design charts accounting for such a high number of independent normalized variables still remains a computationally demanding task. It was therefore decided to fix two normalized variables by attributing commonplace values to them, and to explore with FE the dependence of the hub stress concentration factor on the remaining three normalized parameters ranging within technically significant intervals.

In particular, since the hub outer radius is often approximately twice the inner radius, see Castagnetti and Dragoni (2005), the normalized parameter r_i/r_o was set to 0.5. In addition, it is noted that the hub filleted radius r appears in two variables, namely Ir/r_i^2 and r/r_i. From the FE predictions of Fig. 3 of Strozzi et al. (2011a), addressing a press fit in the absence of shaft bending, it emerges that the hub stress concentration factor strongly depends on the variable Ir/r_i^2, whereas it is considerably less depending on the ratio r/r_i, provided that the considered interval of the normalized fillet radii is not too wide. Since r/r_i is often comprised within the technically sufficiently wide interval 0.025–0.15, see Strozzi et al. (2011a), it was decided to set r/r_i to the intermediate value 0.05, as in Strozzi et al. (2011a).

The effect of the remaining three normalized variables Ir/r_i^2, r_i/l, $Cr_i^2/(IEJ_s)$ has been summarized in the five Figs. 7–11, reporting along the y-axis the hub stress concentration K_t, defined as the hub maximum von Mises equivalent stress normalized over the reference contact pressure p_0, and along the x-axis the normalized parameter Ir/r_i^2, whose relevance has been evidenced in Strozzi et al. (2011a). The parameter Ir/r_i^2 covers the technically significant interval between 10^{-6} and 10^{-2}. Five selected

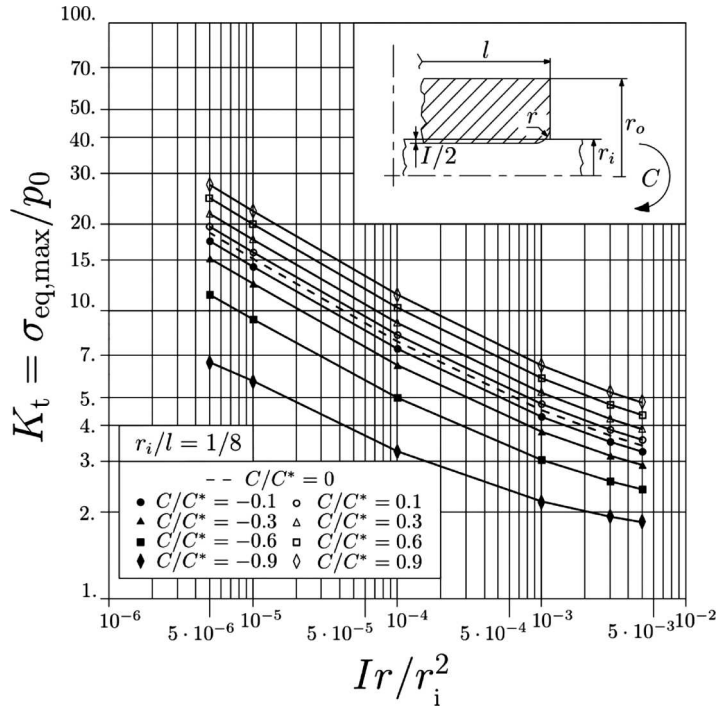

Figure 7. Hub stress concentration K_t in terms of Ir/r_i^2, for $r_i/r_o = 0.5$, $r_i/l = 1/8$, and for a selection of $Cr_i^2/(\text{IEJs})$ values.

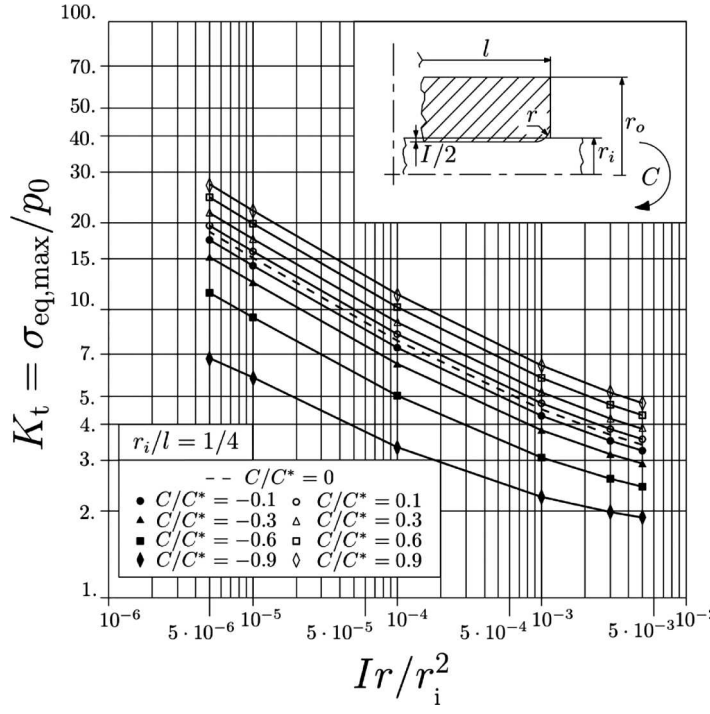

Figure 8. Hub stress concentration K_t in terms of Ir/r_i^2, for $r_i/r_o = 0.5$, $r_i/l = 1/4$, and for a selection of $Cr_i^2/(\text{IEJs})$ values.

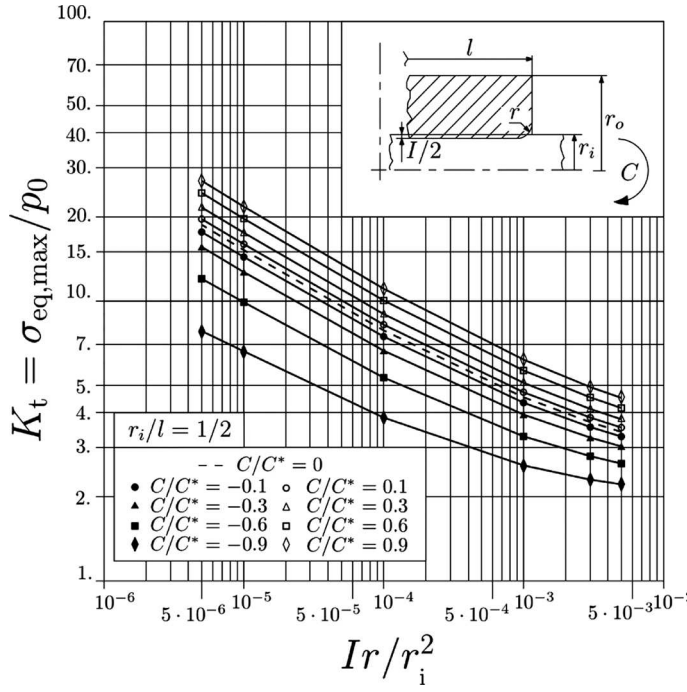

Figure 9. Hub stress concentration K_t in terms of Ir/r_i^2, for $r_i/r_o = 0.5$, $r_i/l = 1/2$, and for a selection of $Cr_i^2/(\text{IEJs})$ values.

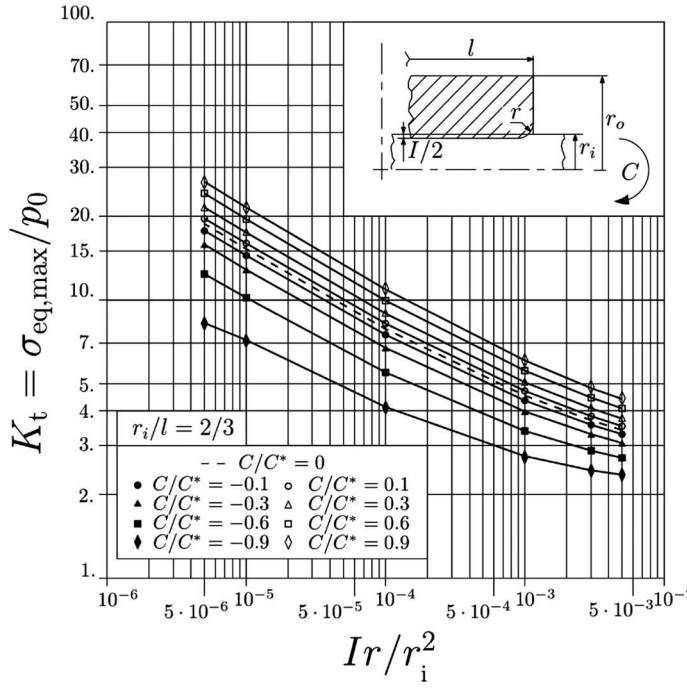

Figure 10. Hub stress concentration K_t in terms of Ir/r_i^2, for $r_i/r_o = 0.5$, $r_i/l = 2/3$, and for a selection of $Cr_i^2/(\text{IEJs})$ values.

values of r_i/l have been considered in Figs. 7–11, namely 1/8, 1/4, 1/2, 2/3, 1; each figure refers to a particular value of r_i/l. A bilogarithmic scale has been adopted.

A family of parametric curves, each referring to a particular value of $Cr_i^2/(\text{IEJs})$, is included in each diagram. The values attributed to $Cr_i^2/(\text{IEJs})$ are expressed as fractions of this variable computed by

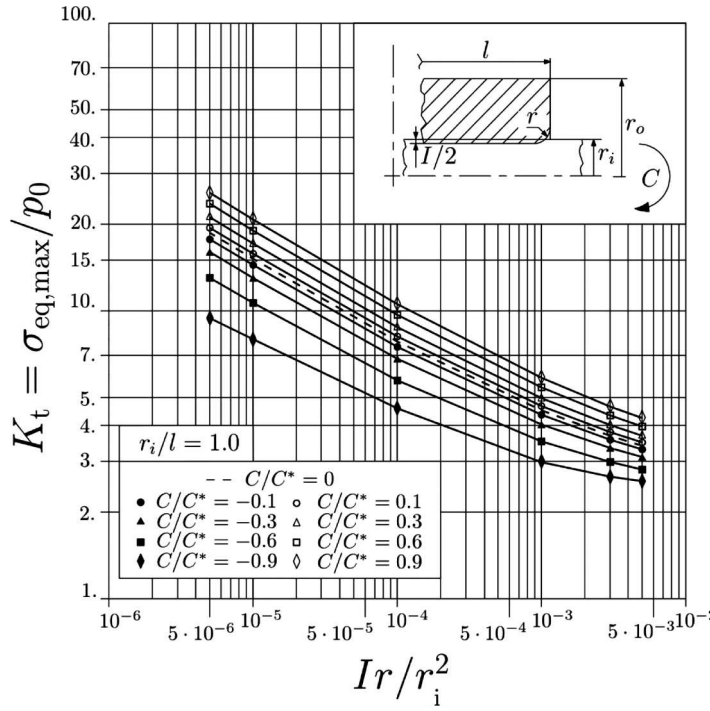

Figure 11. Hub stress concentration K_t in terms of Ir/r_i^2, for $r_i/r_o = 0.5$, $r_i/l = 1$, and for a selection of $Cr_i^2/(\text{IEJs})$ values.

attributing to C its critical value C^* initiating the shaft-hub detachment in a sharply edged, otherwise similar hub, see Section 6. In particular, the values attributed to $Cr_i^2/(\text{IEJs})$ are 0, ±10, ±30, ±60, ±90% of $C^*r_i^2/(\text{IEJs})$. In the diagrams, the following notation is used: if C/C^* is equal to, say, 0.1, this means that the applied normalized couple $Cr_i^2/(\text{IEJs})$ is 10% of its critical value $C^*r_i^2/(\text{IEJs})$ initiating the shaft-hub detachment in a sharply edged hub.

Consequently, these diagrams quantify the increase with respect to a null C of the hub stress concentration K_t in the shaft concave side, due to the presence of a bending couple whose value is, say, 10% of the critical bending couple. Analogously, a negative value of C/C^* equal to, say, -0.1, indicates that the applied normalized couple $Cr_i^2/(\text{IEJs})$ is still 10% of the critical value $C^*r_i^2/(\text{IEJs})$ initiating the shaft-hub detachment in a sharply edged hub, but the reported hub stress concentration K_t is evaluated in the shaft convex side, i.e., in a hub zone antipodal to the previous one, where its value is lower than that referring to a null C. Consequently, these diagrams also quantify the decrease with respect to a null C of the hub stress concentration K_t in the shaft convex side, due to the presence of a bending couple whose value is, say, 10% of the critical bending couple. See also the description of the two K_t values, referring to two hub antipodal positions, reported in Table 1.

Figures 7–11 show that, as a result of the nonlinear character of this contact problem, Strozzi et al. (2011a), the hub stress growth at the shaft concave side, due to the application of a bending couple, is lower than the hub stress decrease at the shaft convex side. The curve for $Cr_i^2/(\text{IEJs}) = 0$ coincides with the predictions of reference Strozzi et al. (2011a), dealing with the press fit stresses in the absence of shaft bending.

In Strozzi et al. (2011a) it has been observed that the maximum equivalent stress within the hub is always higher than its counterpart within the shaft, since the hub stress state is more deviatoric. For this reason, only the hub equivalent stress has been reported in the diagrams.

8. The stress fatigue cycle at the hub contact extremities

The maximum equivalent stress is generally a valid indicator of the stress level in static situations, but not necessarily in the presence of fatigue cycles. However, in some specific problems, the equivalent

stress concept retains its usefulness in fatigue situations too, see e.g. Strozzi et al. (2006) and Strozzi et al. (2011b). Moving to the title problem, since stress fluctuations take place as a result of the shaft bending and of its rotation, the question arises whether the design diagrams of Section 7, reporting the hub maximum von Mises equivalent stress, are still applicable to this fatigue cycle. This point is discussed in the following.

First, it is recalled that the hub stress field referred to in the compilation of Figs. 7–11 ignores the torque applied to the shaft (which, if present, would produce a shear stress $\tau_{a\theta}$, where the indices a and θ denote the axial and circumferential directions, respectively) and it adopts a null coefficient of friction (which, if not null, would produce a shear stress $\tau_{r\theta}$, where the index r denotes the radial direction, as well as a shear stress τ_{ra}). An inevitably approximate discussion on the relative importance of such shear stresses with respect to the stresses accounted for in Figs. 7–11, that is, in the absence of torque and of friction, is presented in the following. For simplicity, this discussion is carried out in the absence of bending couple.

In the design phase, the torque transmissible by the coupling is effectively predicted by the Lamé solution, which correctly describes the central, flattish portion of the shaft-hub contact pressure, and it ignores the torque, the frictionally induced deformations, and the lateral pressure bumps. In fact, while several studies are available that quantify the pressure bump intensity, the effect of the torque and of its frictionally induced deformations is generally neglected, since the corresponding stresses are implicitly assumed as limited, and the torque-induced deformations do not modify the pressure profile, see Strozzi et al. (2011a). In the following, an attempt is made to rationalize these omissions.

The transmissible torque is estimated by supposing that the central contact pressure holds for the whole contact length, and that the shear stress $\tau_{r\theta}$ is obtained by multiplying the uniform contact pressure by a frictional coefficient often lower than 0.2. Since the hub stress field employed to compile Figs. 7–11 refers to the lateral pressure bumps and not to the pressure central part, it may be argued that the nominal value of $\tau_{a\theta}$ is considerably lower than the highest stresses accounted for in the design diagrams.

It may additionally be observed that the local $\tau_{a\theta}$ in the vicinity of the rounded edge is indirectly limited by the frictional threshold, since $\tau_{a\theta}$ is null on the hub frontal faces, and it axially increases as a consequence of the accumulation of the $\tau_{r\theta}$ frictional action, which is bounded. More precisely, the studies addressing the stick-slip zones in a shaft-hub press fit, see Ast et al. (1998) and Savietto et al. (2012), indicate that slip initiates from the shaft-hub contact extremities. Consequently, in such zones the shear stresses $\tau_{r\theta}$ and τ_{ra} cannot exceed their frictional threshold.

It is finally noted that, in shrink fit (as opposed to press fit) assemblies, the shear stress τ_{ra} distributed along the surface of the hub bore is oriented from the contact centre outwards; consequently, the surface of the hub deflects in a convex fashion, and this bending action removes load to the extremities of the contact region with respect to the situation of null τ_{ra}. The above mechanical interpretation has been proposed in Mather and Baines (1972) with regard to the concave deflection of a hollow shaft due to τ_{ra}. This mechanical interpretation may also explain why, in particular situations, the highest values of the stresses have been found at the contact centre and not at the contact edges, Bhonsle and Work (1970). In conclusion, the assumption of null τ_{ra} should be acceptable.

It may be concluded that the three above shear stresses may be neglected in a preliminary stress analysis of the shaft-hub press fit. The above discussion therefore justifies the design diagrams of Section 7 having been compiled by ignoring the effect of torque and friction, a simplifying assumption, this, usually adopted in the majority of the papers dealing with the shaft-hub press fit.

Moving to the stress analysis which the design diagrams of Section 7 are based upon, that is, in the absence of torque and friction, but in the presence of an interference and of a bending couple, it is recalled that only situations have been explored of bending couples not strong enough to (a) locally annul the pressure due to the press fit, and (b) to initiate a detachment between the shaft and the hub. Consequently, the nonlinearities caused by a significant regression of the shaft-hub contact, examined in Section 6 and in Figs. 5 and 6, do not affect the design diagrams of Section 7.

The observations regarding the applicability to fatigue situations of the design diagrams of Section 7 are regrouped into two parts. The first part addresses the shaft-hub contact in the absence of a bending

couple, which constitutes an axisymmetric problem, whereas the second part deals with the shaft-hub contact in the presence of a bending couple, which requires a three-dimensional modeling.

Starting from the axisymmetric problem, the shaft-hub press fit in the presence of an initial interference but in the absence of a bending couple, is progressive with the imposed interference, and, therefore, it is nonlinear, see Strozzi et al. (2011a). However, the numerical forecasts indicate that such behavior is only moderately nonlinear. In particular, the stress components in the zone where the maximum equivalent stress occurs, remain reasonably proportional among them as the interference is increased, and the loci where the maximum equivalent stress falls, move gradually with the shaft-hub interference adopted. That the nonlinearities due to the contact progressive behavior are weak, is confirmed by the recent analytical-numerical results achieved for a plane strain analogue of the axisymmetric shaft-hub press fit, Strozzi et al. (2014).

Moving to the three-dimensional modeling of a shaft-hub press fit in the presence of a bending couple and of an initial interference, it is recalled that the effect of the couple is to increase (lower) the stress components in the shaft concave (convex) side, with respect to its axisymmetric counterpart (i.e., in the presence of an interference but in the absence of a bending couple).

In this case too the numerical forecasts indicate that the stress components in the zone where the maximum equivalent stress occurs, remain reasonably proportional among them as the bending couple is increased. In other words, limiting ourselves to the zone where the bending couple intensifies the stresses with respect to its axisymmetric counterpart, the stress growth due to an increase of the bending couple is similar to the stress growth due to an increase of the initial interference, in the sense that in both cases the stresses raise by remaining reasonably proportional among them, and by maintaining the same proportionality coefficients for the axisymmetric and for the three-dimensional problems. In fact, the two stress fields, activated by (a) the interference, and (b) the bending couple, are kindred by the circumstance that the stress field (a) remains constant in the circumferential direction, whereas the field (b) changes smoothly in the circumferential direction; consequently, they both may be likened to plane strain situations, for which the above proportionality has recently been confirmed in Strozzi et al. (2014). The above similarity is detailed for a particular case in Fig. 12, discussed below.

From Table 1 it is possible to appreciate the deviation from linearity for a particular case, by extracting the two K_t values addressing the two antipodal, reference positions, namely 10.583 and 4.618, by computing their mean value, 7.60, and by comparing this average to the K_t value addressing the null bending couple situation, 7.873. The relative mismatch between the mean value and its null couple counterpart quantifies the deviation from linearity; for this particular problem, this indicator is as low as 3.5%.

The above discussion clarifies that the stress cycle originated by the shaft rotation and due to the initial interference and to the bending couple, may be interpreted to be defined by a mean part engendered by the interference alone, and by an alternating part generated by the bending couple inversion; in addition, the stress components fluctuate by remaining reasonably proportional among them.

By accepting the previously discussed linear approximation, the stress fatigue cycle may be treated as a proportional loading, a situation, this, in which the equivalent stress concept is still applicable to fatigue problems, e.g. Socie et al. (2000). The equivalent uniaxial fatigue cycle may thus be estimated by assuming an equivalent uniaxial mean value defined as the maximum von Mises equivalent stress for the axisymmetric case, that is, in the presence of interference but in the absence of bending couple, see Strozzi et al. (2011a) and Strozzi et al. (2012), whereas the equivalent uniaxial alternating value may be estimated as the difference between the maximum equivalent stress due to both interference and bending couple, which may be extracted from the design diagrams of Section 7, and the maximum equivalent stress for the axisymmetric case. Here the definition is adopted according to which the alternating stress is the difference between the maximum stress and its mean value.

An alternative approach that does not rely on the proportional loading hypothesis is discussed in the following with reference to Case 1 of Table 1, for which a detailed FE stress history investigation has been carried out. Such investigation allows the reliability of the previous simplified approach to be assessed.

In particular, the stress variation has been explored that is promoted by the alternating bending moment due to the shaft rotation, combined with the reference interference. A parallel investigation has

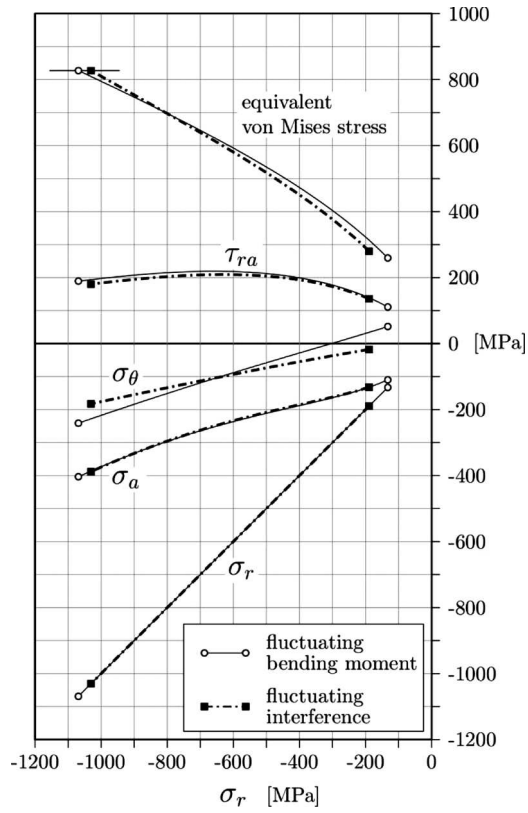

Figure 12. Stress components at the point where the maximum equivalent stress occurs, for a fluctuating bending moment, and for a fluctuating interference.

been carried out by considering a fictitious fluctuation of the interference, whose bounds are selected so that the extremal values of the equivalent stress coincide with those of the previous study. Although this second analysis is purely academic, it allows the comparison of the stress field variation at the pressure bump due to an increase of either the bending moment or of the interference.

In summary, two parallel FE studies have been carried out, namely: (a) a fluctuating loading due to the bending moment, combined to a steady loading due to the initial interference; (b) a fluctuating loading due to the interference, whereas the bending moment is null.

Figure 12 collects the FE forecasts of the two above studies; the four stress components σ_r, σ_a, σ_θ, τ_{ra} ($\tau_{r\theta}$ and $\tau_{\theta a}$ are null due to symmetry), computed at the location where the maximum equivalent stress falls during the cycle, have been plotted versus the reference stress component σ_r.

From the FE predictions it emerges that the curves referring to the two studies are generally essentially superposed, where the maximum discrepancy occurs for σ_θ.

The fact that the stress curves of Fig. 12 may approximately be interpreted as linear from the origin, where the maximum errors occur for the τ_{ra} and σ_θ components, justifies the previously proposed proportional loading assumption. It should also be noted that, while the stress curves referring to the interference alone vanish with the interference itself, the stress σ_θ, computed for the value of the bending moment causing an incipient detachment, does not necessarily vanish with σ_r. This observation rationalizes the fact that the two σ_θ curves are only approximately superposed.

The following observations address the alternative, Dang Van type approach, that is suitable for assessment purposes, since it does not require the proportional loading hypothesis. Such criterion involves two distinct stress indicators of the fatigue cycle, namely the mean hydrostatic stress component, and a suitable alternate shear stress term.

The hydrostatic stress component being compressive during the whole fatigue cycle—a condition common to many Hertzian-like loadings—a preliminary fatigue assessment may be performed by

conservatively neglecting the relieving influence of such compressive component, and by focusing on the remaining indicator. In fact, such relieving influence has been questioned in situations comparable to the title problem. For instance, in Desimone et al. (2005), in the case of a rolling contact fatigue assessment, a modified Dang Van criterion has been applied that ignores the supposedly positive effect of the hydrostatic term if compressive in nature.

Following the above criterion, the fatigue assessment may exclusively be evaluated on the basis of the usual Dang Van alternate shear stress term, described in Dang Van et al. (1989); in brief, such term is computed by removing from the instantaneous deviatoric tensors a mean counterpart, and by extracting from the residual terms a maximum equivalent Tresca shear stress value.

For the case under scrutiny, it has been verified that the mean deviatoric tensor is equal to the average of the two extremal cycle tensors; such behavior is characteristic of proportional cycles, but it also holds for the cycle encountered in this study, which exhibits a sufficiently small deviation from proportionality.

It has been found that the value of the Dang Van alternate shear stress term, which is the significant damage criterion according to Desimone et al. (2005), when the mean hydrostatic stress is compressive, is 35 percent higher than its counterpart derived from the two equivalent von Mises stress values retrieved from the diagrams in the cases of (a) simultaneous application of bending moment and interference, (b) application of interference only. Such derived shear stress term is obtained as the difference between the two above values, scaled by the usual v3 term relating the pure shear stress case and its von Mises equivalent stress value.

The deviation between the two damage indicators, i.e. the Dang Van and the simplified von Mises type approach, does not appear to vary significantly with the applied moment; in fact, by applying two bending moments which are either one third or one sixth of that of Table 1, the actual Dang Van alternate shear stress is respectively 35 and 31% higher than the von Mises derived counterpart.

Such deviation is conceivably ascribable to three concurring effects: (i) the loading is not strictly proportional, and in particular the von Mises equivalent stress fluctuation amplitude underestimates the equivalent value of the stress component amplitude; (ii) a pair of mean ($C/C^* = 0$) and maximum (actual C/C^* ratio) von Mises values retrieved from Figs. 7–11 refer to two different, although near, sub-superficial points, where the maximum equivalent stress falls in the two cases; (iii) the equivalent stress formulations involved are different.

An error as high as 35% is not unfrequently met in the multiaxial fatigue realm; for instance in Foletti et al. (2014), Fig. 12, the modified Dang Van criterion as proposed in Desimone et al. (2005) and favored in this paper is tested versus experimental rolling contact fatigue data; a comparable deviation is perceivable both among the theoretical predictions, and between predictions and measurements.

As a final remark, although in this nonlinear contact problem the fluctuating fatigue cycle does not strictly coincide with its rotating analogue, FE investigations have clarified that the two load conditions produce numerically indistinguishable forecasts.

It may be concluded that the design diagrams of Section 7 retain their usefulness in estimating an equivalent uniaxial fatigue cycle, and that they are applicable, although in an approximate fashion, to forecast a possible fatigue damage.

The previous error analysis has been carried out with reference to a specific fatigue cycle. A detailed investigation of the error incurred in applying this approximate fatigue analysis for a general situation is beyond the scope of this paper.

Future extensions of this paper include the analysis of the frictional effects, e.g. Michalowski and Gawecki (1996), fretting fatigue considerations, e.g. Wang et al. (2006), the analysis of shaft-hub contact profiles more evolved than those described by a flat portion surrounded by two rounded zones, e.g. Kwak and Lee (2009), and the effect of localized sliding zones between the hub and the shaft due to the application of torque, Kim (2011).

9. Conclusions

The elastic stress concentrations developed from the keyless frictionless press fit of a shaft subjected to bending into a hub with rounded bore edges have been addressed. Derived from a formal modeling of the title problem in terms of an integral equation, a set of five normalized parameters has been obtained that

accounts for the combined effects on the hub stress concentration of the fillet radius, the shaft radius, the hub outer radius, the hub axial length, the interference, the Young's modulus, and the bending couple. A numerical validation of the normalized parameters has been presented in tabular form. With the aid of Finite Elements, various design charts have been compiled that (a) forecast the bending couple initiating the detachment between the shaft and the hub, and (b) report the elastic stress concentrations within the hub versus the proposed normalized parameters in the absence of shaft-hub detachment. Such charts assist the designer in correctly dimensioning an interference fit in the presence of a bending couple.

References

Antoni, N. (2014). A study of contact non-linearities in pin-loaded lugs: Separation, clearance and frictional slipping effects. *International Journal of Non-linear Mechanics* 58:258–282. doi:10.1016/j.ijnonlinmec.2013.09.007

Ast, M., Rösle, H., Schenk, R. (1998). *FEM-analyse reibschlüssiger welle-nabe-verbindungen. VDIBerichte 1384, 'Welle-Nabe-Verbingunen—Systemkomponenten im Wandel'*. Fulda, Germany, ISBN 3-18-091384-3. 227–244.

Bhonsle, S. R., Work, C. E. (1970). Evaluation of three dimensional stresses in shrink-fit problems by scattered-light photoelasticity. *Experimental Mechanics* 10(3):19–28N. doi:10.1007/bf02325121

Castagnetti, D., Dragoni, E. (2005). Optimal aspect ratio of interference fits for maximum load transfer capacity. *The Journal of Strain Analysis for Engineering Design* 40(2):177–184. doi:10.1243/030932405×7737

Ciavarella, M., Hills, D. A., Monno, G. (1998). The influence of rounded edges on indentation by a flat punch. *Proceedings of the Institution of Mechanical Engineers, Part C: Journal of Mechanical Engineering Science* 212(4):319–327. doi:10.1243/0954406981521259

Croccolo, D., De Agostinis, M., Vincenzi, M. (2012). Normalisation of the stress concentrations at the rounded edges of a shaft–hub interference fit: Extension to the case of a hollow shaft. *The Journal of Strain Analysis for Engineering Design* 47(3):131–139. doi:10.1177/0309324712439982

Dang Van, K., Griveau, B., Message, O. (1989). On a new multiaxial fatigue limit criterion: Theory and application, biaxial and multiaxial fatigue. *Mech. Eng. Pub EGF* 3:479–496.

Desimone, H., Bernasconi, A., Beretta, S. (2005). On the application of Dang Van criterion to rolling contact fatigue. *Wear* 260(4):567–572. doi:10.1016/j.wear.2005.03.007

Foletti, S., Beretta, S., Tarantino, M. G. (2014). Multiaxial fatigue criteria versus experiments for small crack under rolling contact fatigue. *International Journal of Fatigue* 58:181–192. doi:10.1016/j.ijfatigue.2013.05.006

Garnett, M. D., Grimm,T. R. (1989). Finite element analysis of interference-fitted shafts subjected to bending. *Comput. Eng. ASME* 2:273–280.

Gutkin, R., Alfredsson, B. (2008). Growth of fretting fatigue cracks in a shrink-fitted joint subjected to rotating bending. *Engineering Failure Analysis* 15(5):582–596. doi:10.1016/j.engfailanal.2007.04.003

GWJ Technology GmbH. (2013). Benutzerhandbuch zur webbasierten Berechnungs software eAssistant. http://www.eassistant.eu/fileadmin/dokumente/eassistant/pdf/Hilfe/Handbuch/eAssistantHandb.pdf:52

Hrylits'kyi, D. V., Krasnyuk, P. P. (1997). Elastic contact of two cylinders. *Materials Science* 33(3):284–292. doi:10.1007/bf02539081

Johnson, K. L. (1987). *Contact Mechanics*. Cambridge, UK: Cambridge University Press.

Kim, H. S. (2011). Torque transmission characteristics of the press fit joint between the aluminum shaft and steel ring with small teeth. *Mechanics Based Design of Structures and Machines* 39(1):100–117. doi:10.1080/15397734.2011.538655

Kwak, B. W., Lee, C. W. (2009). Contact analysis by shape optimization (CASO). *Mechanics Based Design of Structures and Machines* 37(2):113–142.doi: 10.1080/15397730902751420

Lee, D. H., Kwon, S. J., Choi, J. B., Kim, Y. J. (2006). Observations of fatigue damage in the press-fitted shaft under bending loads. *Key Engineering Materials* 326(2):1071–1074. doi:10.4028/0-87849-415-4.1071

Madia, M., Beretta, S., Zerbst, U. (2008). An investigation on the influence of rotary bending and press fitting on stress intensity factors and fatigue crack growth in railway axles. *Engineering Fracture Mechanics* 75(8):1906–1920. doi:10.1016/j.engfracmech.2007.08.015

Mather, J., Baines, B. H. (1972). Distribution of stress in axially symmetrical shrink-fit assemblies. *Wear* 21(2):339–360. doi:10.1016/0043-1648(72)90008-7

Michalowski, R. L., Gawecki, A. (1996). Limit torque for a frictional joint. *Mechanics of Structures and Machines* 24(4):499–512. doi:10.1080/08905459608905275

Savietto, P., de Souza, M. M., Savoy, J. (2012). Stick-slip analysis on press-fit joints through finite element method and laboratory tests. SAW Technical Paper No. 2012-36-0189. SAE International, Warrendale, PA, USA. doi:10.4271/2012-36-0189

Socie, D. F., Darrell, F., Marquis, G. B. (2000). *Multiaxial Fatigue*. Warrendale, PA: Society of Automotive Engineers. 484.

Strozzi, A. (2012). A note on the Legendre series solution of the biharmonic equation for cylindrical problems. 108(1):119–123. doi:10.1007/s10659-011-9353-2

Strozzi, A., Baldini, A., Giacopini, M., Bertocchi, E., Bertocchi, L. (2011a). Normalization of the stress concentrations at the rounded edges of a shaft-hub interference fit. *The Journal of Strain Analysis for Engineering Design* 46(6):478–491.

Strozzi, A., Baldini, A., Giacopini, M., Bertocchi, E., Bertocchi, L. (2011b). Maximum equivalent stress in a pin-loaded lug in the presence of initial clearance. *The Journal of Strain Analysis for Engineering Design* 46(8):760–771. doi:10.1177/0309324711423587

Strozzi, A., Baldini, A., Giacopini, M., Bertocchi, E., Bertocchi, L. (2012). November. Stress concentrations at the rounded edges of a shaft-hub interference fit. ASME 2012 Mechanical Engineering Congress, Houston, Texas.

Strozzi, A., Baldini, A., Giacopini, M., Bertocchi, E., Bertocchi, L. (2013). Achievement of a uniform contact pressure in a shaft–hub press-fit. *Proceedings of the Institution of Mechanical Engineers, Part C: Journal of Mechanical Engineering Science* 227(3):405–419. doi:10.1177/0954406212461994

Strozzi, A., Baldini, A., Nascimbeni, M. (2006). Maximum equivalent stress in a pin-loaded lug subject to inclined loading. *The Journal of Strain Analysis for Engineering Design* 41(4):297–309. doi:10.1243/03093247jsa150

Strozzi, A., Bertocchi, E. (2015). A note on the Legendre series solution of the Laplace equation for cylindrical problems. *Journal of Elasticity* 118(1):109–112. doi:10.1007/s10659-014-9476-3

Strozzi, A., Bertocchi, E., Baldini, A., Giacopini, M. (2014). On the applicability of the Boussinesq influence function in modelling the frictionless elastic contact between a rectangular indenter with rounded edges and a half-plane. *Proceedings of the Institution of Mechanical Engineers, Part C: Journal of Mechanical Engineering Science* 229:987–1001. doi:10.1177/0954406214542641

Wang, R. H., Jain, V. K., Mall, S., Sabelkin, V. (2006). Enhancement of fretting fatigue strength through stress-relieving slot. *Mechanics Based Design of Structures and Machines* 34(2):113–138. doi:10.1080/15397730600640404

White, D. J., Humpherson, J. (1969). Finite-element analysis of stresses in shafts due to interference-fit hubs. *The Journal of Strain Analysis for Engineering Design* 4(2):105–114. doi:10.1243/03093247v042105